2012

Magnetic hyperthermia investigation of cobalt ferrite nanoparticles: Comparison between experiment, linear response theory, and dynamic hysteresis simulations

JOURNAL OF APPLIED PHYSICS, MELVILLE, v. 111, n. 12, pp. 49-56, 2012
http://www.producao.usp.br/handle/BDPI/42578

AIP | Journal of Applied Physics

Magnetic hyperthermia investigation of cobalt ferrite nanoparticles: Comparison between experiment, linear response theory, and dynamic hysteresis simulations

E. L. Verde, G. T. Landi, J. A. Gomes, M. H. Sousa, and A. F. Bakuzis

Citation: J. Appl. Phys. **111**, 123902 (2012); doi: 10.1063/1.4729271
View online: http://dx.doi.org/10.1063/1.4729271
View Table of Contents: http://jap.aip.org/resource/1/JAPIAU/v111/i12
Published by the American Institute of Physics.

Magnetic hyperthermia investigation of cobalt ferrite nanoparticles: Comparison between experiment, linear response theory, and dynamic hysteresis simulations

E. L. Verde,[1,2] G. T. Landi,[3] J. A. Gomes,[4] M. H. Sousa,[5] and A. F. Bakuzis[1,a)]
[1]*Instituto de Física, Universidade Federal de Goiás, 74001-970 Goiânia-GO, Brazil*
[2]*Instituto de Ciências Exatas e da Terra, Universidade Federal de Mato Grosso, 3500, Pontal do Araguaia-MT, Brazil*
[3]*Instituto de Física, Universidade de São Paulo, 05314-970 São Paulo-SP, Brazil*
[4]*Instituto de Criminalística, Polícia Civil do Distrito Federal, 70610-200 Brasília-DF, Brazil*
[5]*Faculdade de Ceilândia, Universidade de Brasília, 72220-140 Brasília-DF, Brazil*

(Received 1 December 2011; accepted 14 May 2012; published online 18 June 2012)

Considerable effort has been made in recent years to optimize materials properties for magnetic hyperthermia applications. However, due to the complexity of the problem, several aspects pertaining to the combined influence of the different parameters involved still remain unclear. In this paper, we discuss in detail the role of the magnetic anisotropy on the specific absorption rate of cobalt-ferrite nanoparticles with diameters ranging from 3 to 14 nm. The structural characterization was carried out using x-ray diffraction and Rietveld analysis and all relevant magnetic parameters were extracted from vibrating sample magnetometry. Hyperthermia investigations were performed at 500 kHz with a sinusoidal magnetic field amplitude of up to 68 Oe. The specific absorption rate was investigated as a function of the coercive field, saturation magnetization, particle size, and magnetic anisotropy. The experimental results were also compared with theoretical predictions from the linear response theory and dynamic hysteresis simulations, where exceptional agreement was found in both cases. Our results show that the specific absorption rate has a narrow and pronounced maxima for intermediate anisotropy values. This not only highlights the importance of this parameter but also shows that in order to obtain optimum efficiency in hyperthermia applications, it is necessary to carefully tailor the materials properties during the synthesis process. [http://dx.doi.org/10.1063/1.4729271]

I. INTRODUCTION

The use of magnetic nanoparticles on biomedical applications has increased considerably in recent years. This new area is being called biomedical nanomagnetics and focuses on local drug targeting, diagnostics, and/or disease therapy.[1] Several applications have been reported, ranging from stem cell labeling, atherosclerosis, or metastasis detection, to cancer treatment.[1–12] Cancer treatment with magnetic nanoparticles is based upon the magnetic hyperthermia phenomenon, which consists of an increase on the temperature of magnetic nanoparticles (heat centers) due to the interaction of their magnetic moments with an alternating magnetic field. The heating process is related to hysteresis losses which are proportional to the hysteresis loop area.[12] At the low-field range, where the response is linear, the loops are always ellipsis and the heating power is given by[9,12]

$$P_m^{LRT} = \pi\mu_0\chi_0 H_0^2 f \frac{2\pi f\tau}{1+(2\pi f\tau)^2}, \quad (1)$$

where χ_0 is the equilibrium susceptibility and $\tau = \tau_0(\pi/\sigma)^{1/2} e^{\sigma}$ is the Néel-Brown relaxation time.[13] Here, $\tau_0 = (2K_{ef}\gamma_0/M_s)^{-1} \sim 10^{-10}$ s and $\sigma = K_{ef}\mathrm{V}/\mathrm{kT}$, where K_{ef} is the effective uniaxial magnetic anisotropy, γ_0 is the electron's gyromagnetic ratio, M_s is the saturation magnetization, V is the particle's volume, k is Boltzmann's constant, and T is the sample temperature. As the field increases, it enables the magnetization to surmount the anisotropy barrier that separates the stable energy minima, thus rendering the magnetic response non-linear. This introduces a new contribution to the energy dissipation which, unfortunately, cannot be described by means of a simple expression. In this case, numerical simulations using the Landau-Lifshitz equation are necessary to better understand the phenomenon.[14–17]

Recently, there has been a considerable effort to optimize materials properties for hyperthermia applications, with the majority of papers focusing on controlling the size dispersion or enhancing the saturation magnetization of the nanoparticles.[1,8–11,18] A possible material for such application is cobalt ferrite, which has both enhanced anisotropy and saturation magnetization. In addition, this nanomaterial has been found to have multifunctional applications spanning from room-temperature spin filtering,[19] multiferroic devices[20,21] to even MRI contrast agents.[22] Moreover, as a ferrite, their magnetic properties (K_{ef} and M_s included) are strongly dependent upon cation distribution or atom-substitution.[23–26] However, although this has been known for some time, usually only the effect of M_s is highlighted, whereas K_{ef} is seldom included as one of the parameters to enhance the heating efficiency. This aspect of the problem

a)Author to whom correspondence should be addressed. Electronic mail: bakuzis@if.ufg.br.

was the subject of recent theoretical[12,16] and experimental[27,28] studies which predicted optimum anisotropy parameters and thus emphasized its importance. Nevertheless, to our knowledge, there is still a lack of experimental investigations on the subject, in particular, concerning the comparison between experimental data and theoretical predictions.

In this paper, we investigate the magnetic hyperthermia properties of cobalt-ferrite nanoparticles with diameters ranging from 3 to 14 nm. Such low particle sizes are interesting since, by reducing aggregation phenomena, one can avoid embolization and colloid stability issues. In fact, for this and other reasons, the interest in this type of material for theranostic (diagnostic and therapeutic) applications is continuously increasing.[22,27–30] On the other hand, a possible restriction to the use of some ferrites, including cobalt-ferrite, has to do with its potential toxicity caused by the leaching of Co atoms from the nanoparticle surface under biological environments.[22,31] Nevertheless, if such issues can be controlled, as for instance through an efficient surface passivation, this system could be interesting, especially at the non-linear regime (high magnetic fields),[6] where a larger magnetic anisotropy is expected to play a significant role. In this work, we show measurements of the specific absorption rate ((SAR); power dissipated per unit mass) as a function of particle size, saturation magnetization, coercive field, and magnetic anisotropy. The data were obtained for fields up to 68 Oe and compared with analytical predictions from the linear response theory (LRT), as well as with numerical simulations of dynamic hysteresis (DH) using the stochastic Landau-Lifshitz equation. The agreement between theory and experiment is noteworthy and our results show that the anisotropy is in fact a prime parameter in the search for materials optimized for magnetic hyperthermia.

II. NANOPARTICLE SYNTHESIS

Nanoparticles were synthesized by forced hydrolysis of Fe^{3+} and Co^{2+} in a coprecipitation procedure[32] divided in three steps, as follows: (i) 50 ml of a solution containing 25 mmol of Fe^{3+} and 12.5 mmol of Co^{2+} was introduced, under vigorous stirring, into 200 ml of 2 mol/l alkaline solution at different temperatures—as specified in Table I—and left for 60 min. The obtained solid was magnetically separated from the supernatant and washed three times with distilled water. (ii) The precipitate was acidified with a 2 mol/l HNO_3 solution, centrifuged and the supernatant discarded. The obtained nanograins were hydrothermally treated with 1 mol/l boiling solution of $Fe(NO_3)_3$ for 30 min and the excess ferric nitrate was removed from the solution by magnetic decantation. (iii) The precipitate was washed three times with acetone, and then any excess acetone was evaporated in order to peptize nanoparticles in water (*p*H of about 2). Powders were obtained from the evaporation of the samples during the different steps of the synthesis. Note that different particle sizes were achieved by using distinct alkaline medium (see Table I).

III. NANOPARTICLE CHARACTERIZATION

Powder x-ray diffraction was performed in a synchrotron source at the Brazilian National Synchrotron Laboratory (LNLS) facility. The results are illustrated in Fig. 1, which shows the diffractogram for sample CD1 (see Table I) together with the Rietveld analysis from which we obtained the particle size as well as the degree of cation distribution of the $Co_xFe_{3-x}O_4$.[33] For most samples x equals 1, which corresponds to an inverted spinel structure. The exceptions are samples CD1 and CD2 where $x = 0.74$ and 0.91, respectively.

The room temperature saturation magnetization was obtained using an ADE Magnetics vibrating sample magnetometer model EV9. The inset in Fig. 2 shows the magnetization curve for some representative samples (CC3, CD1, and CA3). The saturation magnetization values were obtained by data extrapolation at the high-field limit (cf. Table I). Fig. 2 shows the magnetization data at low field range for the same samples, from which the coercive field (H_C) was extracted. The results are summarized in Figure 3, which presents the coercive field as function of particle size for all samples studied. As expected, the samples with smaller diameter (CA3 and CB3) are in the superparamagnetic regime, which is expected to remain up to a critical value called the superparamagnetic diameter (D_{SP}). Above this value thermal stability sets in at a rate proportional to the volume (D^3), and thus a steep increase in the coercivity is observed.

Further, the effective magnetic anisotropy was calculated from H_C considering a three dimensional random anisotropy axis coercive field (H_c^{3D})[34] and taking into account

TABLE I. Cobalt-ferrite powder samples parameters.

	Rietveld analysis				Synthesis conditions	
Name	Diameter (nm)	M_s (emu/cm^3)	H_c (Oe)	K_{ef} (10^5 erg/cm^3)	Base; temperature	Step[a]
CA3	3.1	121.8	0.6	3.54[b] (5.51[b,c])	NH_4OH; 25 °C	iii
CB3	3.4	102.5	1.4	3.54[b] (5.51[b,c])	NH_4OH; 100 °C	iii
CC1	8.4	249.1	219.4	4.84 (8.25[c])	$(CH_3)NH_2$; 100 °C	i
CC3	9.1	271.9	152.5	2.77 (4.33[c])	$(CH_3)NH_2$; 100 °C	iii
CD1	12.9	253.3	261.3	2.64 (4.42[c])	NaOH; 100 °C	i
CD2	13.6	280.9	298.7	3.22 (4.87[c])	NaOH; 100 °C	ii
CD3	13.5	314.5	347.9	4.22 (5.70[c])	NaOH; 100 °C	iii

[a]Step in which powders were obtained.
[b]Mean anisotropy value.
[c]Core-shell correction.

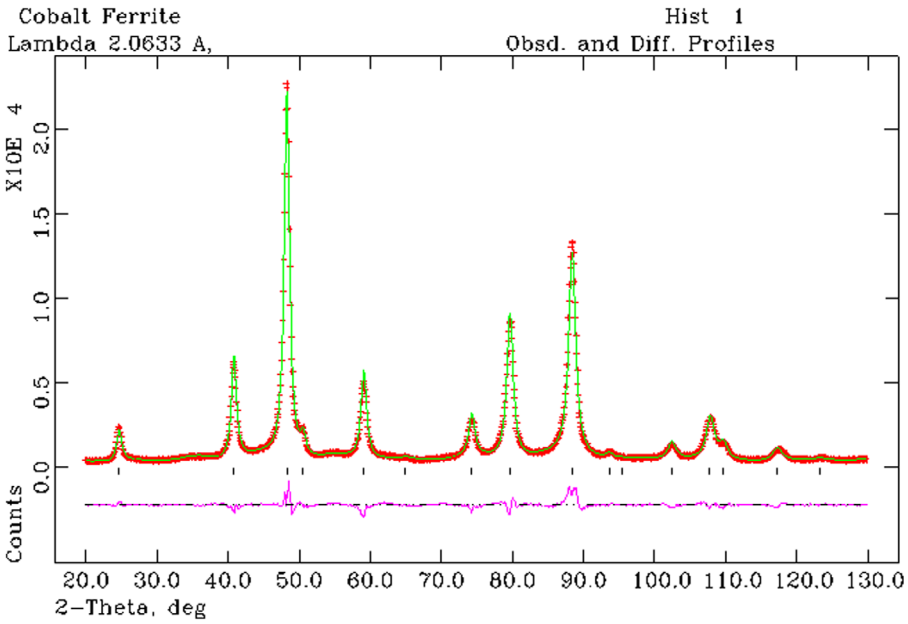

FIG. 1. Rietveld refinement pattern of sample CD1. The lower curve represents the difference between the observed and calculated profiles. Plus (+) marks represent the collected data and tick marks show the positions for the allowed reflections. The agreement factors for x-ray diffraction obtained from the Rietveld analysis were $R\text{p} = 5.47\%$, $R\text{wp} = 6.70\%$, and $\chi^2 = 6.606$.

particle-particle interactions.[35] That is, the experimental coercive field is equal to the isolated nanoparticle coercivity (H_c^{3D})[34] times an interaction term which is proportional to the packing fraction (p) of the nanoparticles, $H_c = H_c^{3D}(1-p)$.[35] Here, we considered that shape anisotropy is the dominant contribution to the magnetic anisotropy of the nanoparticles. Such assumption comes from the fact that several ferrite-based nanoparticles in this size range has shown an effective uniaxial magnetic anisotropy.[36–38] In this situation, one can show that K_{ef} can be calculated from

$$K_{ef} = \frac{M_s * H_c}{0.96 * \left[1 - \left(\frac{D_{sp}}{d}\right)^{2.25}\right](1-p)}, \qquad (2)$$

where we considered a packing fraction of p = 0.65 (which is a value between 0.634 for the random close packing of spheres and 0.659 for the unequal sphere packing of a bidisperse system), while the superparamagnetic diameter (D_{SP}) was obtained from the data analysis, i.e., 7 nm. The values of

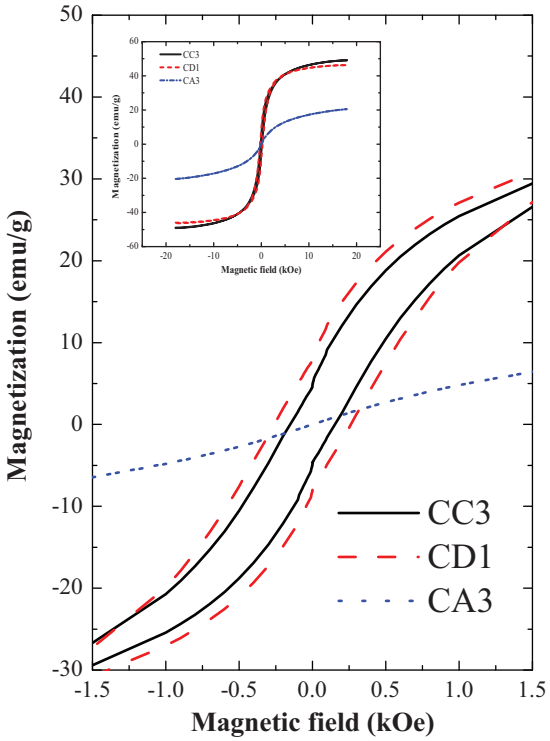

FIG. 2. Magnetization curves for samples CA3, CD1, and CC3 at a low field range. In the inset is shown the room temperature magnetization curves for the same samples at the whole field range.

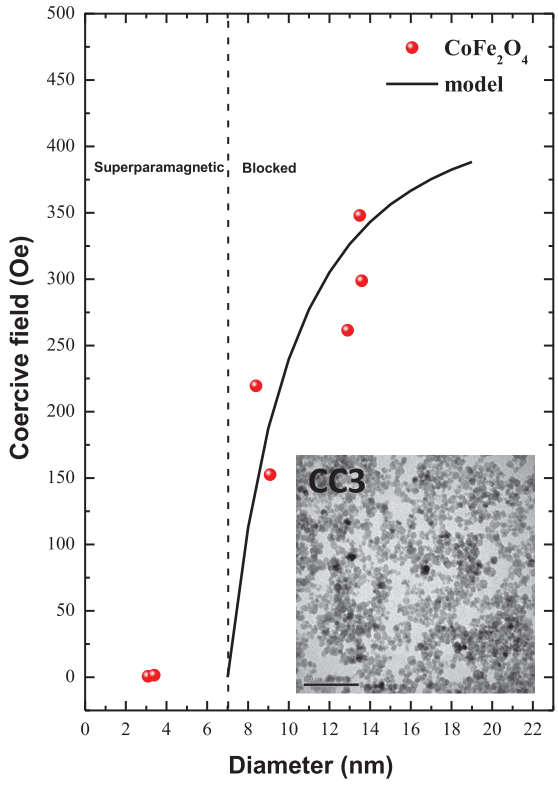

FIG. 3. Coercive field as function of particle size for all samples. Symbols represent experimental data whereas the solid line was calculated from Eq. (2).

K_{ef} are shown in Table I and were found to lie in the range of 2.6–4.9 $\times 10^5$ erg/cm^3, which is slightly lower than the bulk value $K_{bulk} = (1 \text{ to } 2) \times 10^6$ erg/cm^3.[9] In fact, in a recent study of Al-substituted cobalt-ferrite nanoparticles, this discrepancy was found to be related to distinct annealing temperatures.[39] Further, the solid line in Figure 3 corresponds to the theoretical calculation using $H_c = H_c^{3D}(1-p)$, where we used the mean values of the effective anisotropy (3.54×10^5 erg/cm^3) and saturation magnetization (273.9 emu/cm^3). As can be seen, the agreement with the experimental data, without any fitting parameters, is excellent. In the inset of Fig. 3, we show a TEM image of sample CC3. The scale bar is 100 nm. One can clearly observe the existence of some non-spherical (anisometric) particles, which, in accordance with our assumption, would be responsible for a shape anisotropy contribution. However, the axial ratio is not very high. Moreover, by randomly choosing 50 nanoparticles from the image in the inset of Fig. 3, using the free software IMAGEJ, we found an axial ratio (r) within the range of 1–2.6. The mean value of r was found to be 1.3 ± 0.3. Indeed, though the results suggest that shape anisotropy is important, we noticed that the theoretical calculations of this term are still lower than the ones obtained experimentally. As for instance, for an axial ratio (r) of 1.2 we obtained $K_{ef} = 0.3 \times 10^5$ erg/cm^3, while for r = 3 one finds $K_{ef} = 1.6 \times 10^5$ erg/cm^3. As a consequence, it is highly possible that other contributions (such as magnetoelastic or surface anisotropy) could be also present. Nevertheless, the inclusion of such terms is not believed to change significantly the values estimated for the effective magnetic anisotropy. (The above calculation was based on the hypothesis of a homogeneous cobalt-ferrite nanoparticle. However, due to the synthesis process, as discussed later in the text, a core-shell nanostructure is more likely to occur. This will also increase the estimated magnetic anisotropy values.)

IV. MAGNETIC HYPERTHERMIA RESULTS AND DISCUSSION

The magnetic hyperthermia experimental set up consists basically of a power supply, a coil (inductor), and a capacitor network (refrigerant cooled—218 nF) that together with the inductor (L-match) forms a resonant circuit. In our system, the working frequency was around 500 kHz and corresponds to a sinusoidal wave. The copper coil length was 10.2 cm with a diameter of 2.2 cm. During the experiment, the coil was cooled using a closed-loop circulating water system. At our experimental conditions, the coil temperature is maintained at room temperature within an error of 0.3 °C. Measurements were performed in an interval of 300 s and the amplitude of the alternating magnetic fields were 22, 45 and 68 Oe, obtained from measurements using an ac field probe. All samples had the same mass (0.090 ± 0.001 g) and were always inserted inside the coil at the same position. The sample temperature is measured with an infrared meter. A data acquisition system converts the analogical signal from the infrared meter to a digital one that is then analyzed in a computer. Fig. 4 shows the temperature variation (ΔT) as function of measuring time for the samples CA3, CC3, and CD1

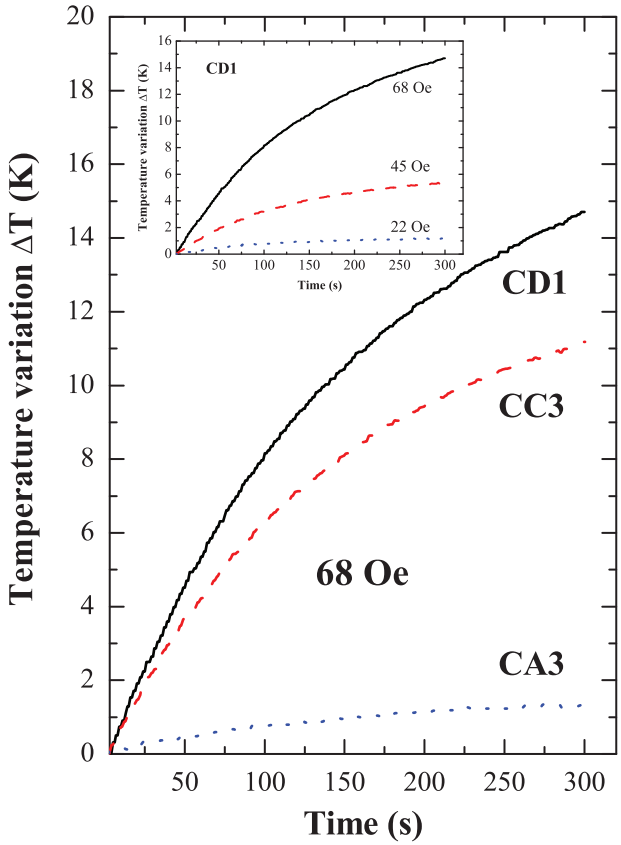

FIG. 4. Temperature variation as a function of time for samples CA3, CC3, and CD1 with an applied field of 68 Oe. The inset shows the same as before for sample CD1, but with different magnetic fields.

with a field of 68 Oe. The inset in the same figure shows again ΔT as function of time but now for sample CD1 with different values of the applied magnetic field. As expected, the higher the field the higher the temperature variation. Note that only powder samples were investigated, so there is no contribution from Brownian relaxation.[9]

The SAR is obtained from the slope of the temperature variation at the initial stage of the process (small times) by means of the following equation: $SAR = \frac{cM}{m}\frac{dT}{dt}$, where $c = 700$ Jkg^{-1}K^{-1} is the sample specific heat (assumed the same as the bulk value[9]—700 Jkg^{-1}K^{-1}), M is the total mass of the sample (in kg) and m is the mass of magnetic nanoparticles (in grams). In Fig. 5, we present results for the SAR as a function of M_s (main figure) and H_C (inset) for different values of the applied field. First and foremost, it is possible to see that the SAR increases with increasing field amplitude, which is expected since more energy is being poured into the system. Indeed, Eq. (1) predicts that in the linear regime, the $SAR \propto H_0^2$.

In order to optimize the SAR, a careful analysis of the combined influence of the parameters appearing in Eq. (1) is necessary. For instance, the dependence on M_S is monotonically increasing and thus justifies the aforementioned interest in enhancing it for hyperthermia applications. However, this is clearly not the case in Fig. 5, where distinct maxima are seen to exist in both graphs. The obvious reason for this discrepancy is the fact that the other parameters are not fixed but vary for each sample. As we now discuss, the anisotropy

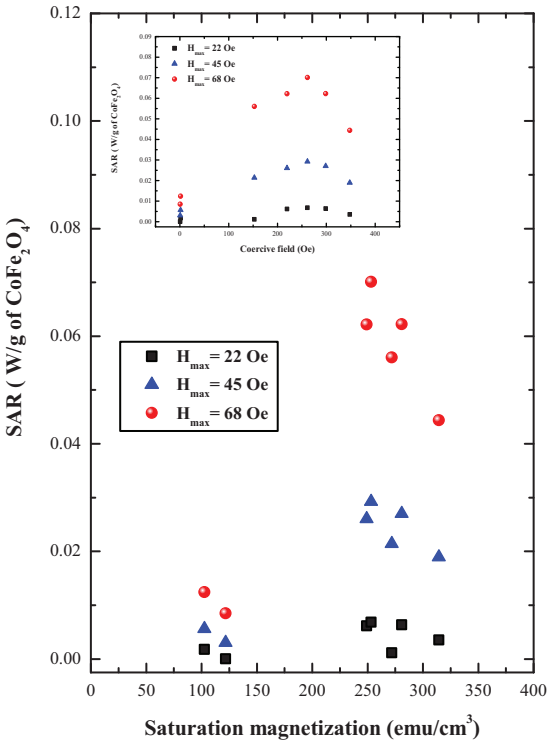

FIG. 5. SAR as a function of saturation magnetization for different values of the applied field. The inset shows SAR as a function of the coercive field for different magnetic fields.

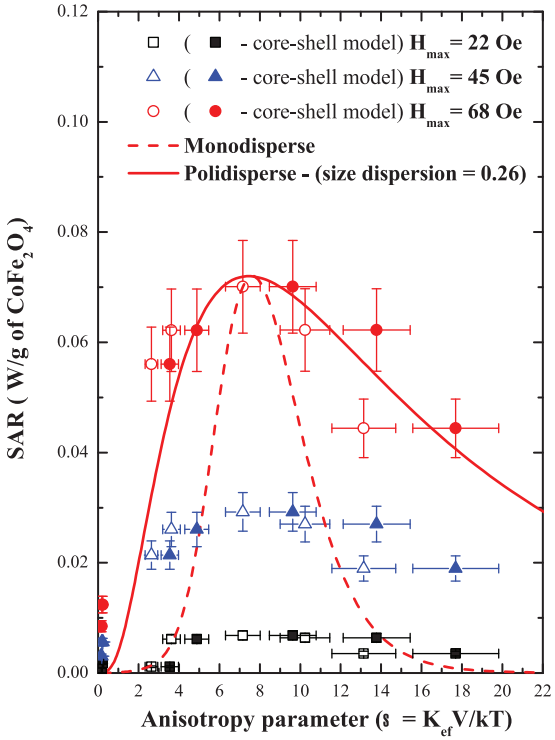

FIG. 6. SAR as a function of the dimensionless magnetic anisotropy parameter $\sigma = K_{ef}\mathrm{V/kT}$ for different values of the applied field. Open (closed) symbols represent experimental data (experimental data taking into account a core-shell nanoparticle), while the dashed (solid) line represent the linear response theory calculation (Eq. (1)) for a monodisperse (polydisperse) nanoparticle system.

is in this sense particularly important. It is simpler, however, to study the dependence in terms the dimensionless anisotropy parameter $\sigma = K_{ef}\mathrm{V/kT}$, with which Eq. (1) may be written in its simplest form. The reason for this is the following: for a fixed frequency and field, the SAR may be expressed, up to a multiplicative factor, solely in terms of σ and τ_0. The latter, in particular, depends explicitly on M_S, as seen from the previously provided expression, $\tau_0 = (2K_{ef}\gamma_0/M_s)^{-1} \sim 10^{-10}$ s. However, this is only an approximation and, indeed, τ_0 is usually regarded as poorly known number due to the experimental uncertainties pertaining to the problem. Thence, to a first approximation we may take τ_0 as constant for all samples, therefore reducing the dependence of the SAR to a single parameter, σ.

Fig. 6 shows the SAR as a function σ for different values of the applied field. Open symbols are the experimental data. The estimated position of the maxima is $\sigma_{\mathrm{m}} = 7.2 \pm 0.9$. We found an increase in the SAR value for higher fields. The dashed line represents calculations using Eq. (1) and $\tau_0 = 5 \times 10^{-10}$ s where the height was adjusted to fit the experimental data. The calculated value for this maximum is $\sigma_m^{LRT} = 7.5$, which agrees well with the experiment, even though the general form of the curves are notably different. It is also worth mentioning that σ_m^{LRT} may be tuned by changing τ_0. For instance, using $\tau_0 = 1 \times 10^{-10}$s we arrive at $\sigma_m^{LRT} = 9.2$. This, however, lacks in physical significance since τ_0 is only an approximate number which, indeed, should be different for each sample. As a next step, motivated by the poor agreement between both curves, we also calculated the contribution from the size distribution (solid line). We considered a log-normal distribution of diameters with a size dispersion of 0.26, which is a typical value obtained using this method of preparation.[40–42] As can be seen, the agreement with the experimental data is now remarkably good showing that Eq. (1) is indeed an adequate expression for the linear regime. This analysis illustrate quite clearly that the SAR is not a simple monotonic function of the anisotropy and that optimum values exist for which it is maximized. Note also that this change is quite sensitive, especially in monodisperse systems where a narrow peak is observed (Fig. 6, dashed line).

For similar particle sizes, the values of the SAR for samples CD1 (12.9 nm), CD2 (13.6 nm) and CD3 (13.5 nm) for 68 Oe were found to be 0.07, 0.06, and 0.04 W/g of cobalt-ferrite, respectively. In this case, the largest value was found for the lower effective magnetic anisotropy, i.e., the lower cation distribution value. Indeed we found for sample CD1 $K_{ef} = 2.6 \times 10^5$ erg/cm^3 and x = 0.7, CD2 $K_{ef} = 3.2 \times 10^5$ erg/cm^3 and x = 0.91, and CD3 $K_{ef} = 4.2 \times 10^5$ erg/cm^5 with x = 1. This result indicates that mixed spinel cobalt ferrite, instead of inverted spinel, are more suited for hyperthermia applications. It also agrees with the linear response theory, which predicts that within a certain range, the SAR should be higher for lower anisotropy materials[12] (see Fig. 6). This information is interesting for low field magnetic hyperthermia applications.

All the later discussions were based upon the assumption of a homogeneous cobalt-ferrite nanoparticle. However, in order to prevent nanoparticle degradation in acidic

medium, step (ii) is introduced during the nanoparticle synthesis (see Sec. II). In this case, a shell rich in Fe^{3+} is formed at the nanoparticle surface, which promotes the formation of a core-shell nanoparticle (expected to be a $CoFe_2O_4$-γ-Fe_2O_3 nanostructure).[43] It is found, for this type of ferrite, that the shell is weakly magnetic and its length decreases the lower the particle size, while the core might be considered with similar properties as the bulk.[43] So, within the core-shell model, one should consider the bulk saturation magnetization of 425 emu/cm^3 in the effective anisotropy calculation (see Eq. (2)), instead of the measured particle magnetization. In Table I, the values of K_{ef} in the parenthesis correspond to the core-shell correction. Note that the effective anisotropy values had increased. In particular, using this model, the shell volume fraction was found to change from 26% for the largest particle size (sample CD3) to 71% for the lowest nanoparticle diameter (sample CA3). Those values are in the range estimated in Ref. 43 and clearly emphasize the role of surface and finite size effects in those nanoparticles. So, with that in mind, one can recalculate the anisotropy parameter σ. In Fig. 6 solid symbols correspond to the core-shell nanoparticle correction. Note that, when compared with the previous calculation (open symbols), a better agreement with the linear response theory is obtained.

Further, in order to better understand the underlying mechanism of magnetic hyperthermia and to study the transition to the non-linear regime, we also performed dynamic hysteresis (DH) simulations. The starting point is the Néel-Brown theory,[13] where in order to account for the influence of temperature, the Landau-Lifshitz equation is augmented with a white noise thermal field satisfying $\langle H_{th}^i(t)H_{th}^j(t')\rangle = \frac{2kT\eta}{V}\delta_{i,j}\delta(t-t')$, with $i,j = x,y,z$. That is,

$$\dot{\boldsymbol{M}} = -\gamma_0\, \boldsymbol{M}\times\boldsymbol{H}_T - \gamma_0\frac{\alpha}{M_s}\boldsymbol{M}\times(\boldsymbol{M}\times\boldsymbol{H}_T), \qquad (3)$$

where γ_0 is the electron's gyromagnetic ratio and α is the dimensionless damping parameter. Here, $\boldsymbol{H}_T$ is the total magnetic field, which comprises the external (Zeeman), anisotropy, and thermal fields. Our approach is based on the solution of the full hierarchy of differential recurrence relations obtained from averaging over the stochastic realizations of Eq. (3). A thorough explanation of the procedure is beyond the scope of this paper and is described in detail in Ref. 15. The relevant point is that the solutions so obtained are free of any approximations enabling us to study with great flexibility the escape from the linear regime as the field amplitude is increased. For simplicity, only monodisperse systems were considered and, in order to mimic real samples, all simulations refer to systems with randomly oriented anisotropy axes. We also fixed f = 500 kHz and $\alpha = 1$. Finally, the field amplitude is given in normalized units, in terms of the anisotropy field $H_A = 2K_{ef}/M_s$; that is, we work with $h_0 = H_0/H_A$.

In Fig. 7(a), we compiled typical hysteresis loops for different values of σ and three distinct magnetic fields. The SAR may be computed immediately from these curves since it is directly proportional to the loop area (A): SAR = fA. As it can be seen, starting at low σ, practically no hysteresis is observed, thus giving a nearly null area. Then, with increasing σ the area first increases, reaches a maximum, and then decreases towards the high anisotropy region. As expected, this behavior is in complete agreement with the results in Fig. 6. It is also interesting to note that the magnetic response at low and high σ are actually quite similar, even though they correspond to completely different physical scenarios. In the former, the volume and/or anisotropy are low enough to enable the magnetization to move with ease between the stable energy states, agitated violently by the thermal fluctuations. On the other hand, in the latter, the very opposite takes place, with the spins being practically blocked ("frozen"), so that only a weak precession near the equilibrium positions may take place.

The values of the magnetic field presented were chosen to illustrate the differences between the linear and non-linear regime. From Fig. 7(a), it can be seen that the elliptic behavior characteristic of the linear regime is gradually lost as the field increases, giving place to more complex non-linear shapes. At low σ, for instance, these resemble Langevin curves characteristic of a superparamagnetic state, which deviate from a straight line as the field gradually increases. The shape of the loops at the non-linear regime is also quite different from square loops reminiscent of the Stoner-Wohlfarth model. The reason for this is the effect of the high-frequency excitation which hampers the magnetic response. Indeed, the actual area of the loop depends in a quite complex manner on the combined values of f and σ, which represent the competition between the gyromagnetic and thermal responses, respectively.

Finally, we present in Fig. 7(b) curves for the SAR/h_0^2 vs. σ calculated for different values of h_0. First and foremost, we emphasize that these results agree precisely with Eq. (1) (see also Fig. 6). Furthermore, they corroborate our previous discussion that, in the linear regime the SAR scales with h_0^2, a fact that is clearly seen to hold until $h_0 = 0.07$. Afterwards, the maxima are seen to get shifted to the right, accompanied by a decrease on the efficiency near the maximum. We emphasize that by efficiency, we refer to the quantity SAR/h_0^2. The SAR itself is obviously considerably larger for higher magnetic fields. We also note that the efficiency may, in general, either decrease or increase. For instance, when $\sigma = 13$ in Fig. 7(b), the efficiency for $h_0 = 0.21$ shows a nearly 8-fold increase compared to its linear counterpart. This follow from the fact that in this region, the particles are blocked and, therefore, able to respond efficiently only to large magnetic fields. Note that using the average correspondence between h_0 and H_0 we have that, using the average values of K_{ef} and M_s obtained from our previous analysis (see Sec. III), we obtain a anisotropy field of $H_A \sim 2830$ Oe. Hence, $h_0 = 0.07$ corresponds to $H_0 \sim 200$ Oe, which is well above the values employed in the experiments discussed. We call attention, however, to the fact that this value is by no means accurate and should be taken simply as a rough estimate. For instance, these simulations do not account for particle-particle interactions which, as discussed in Sec. III, are expected to play a significant role in the system investigated.

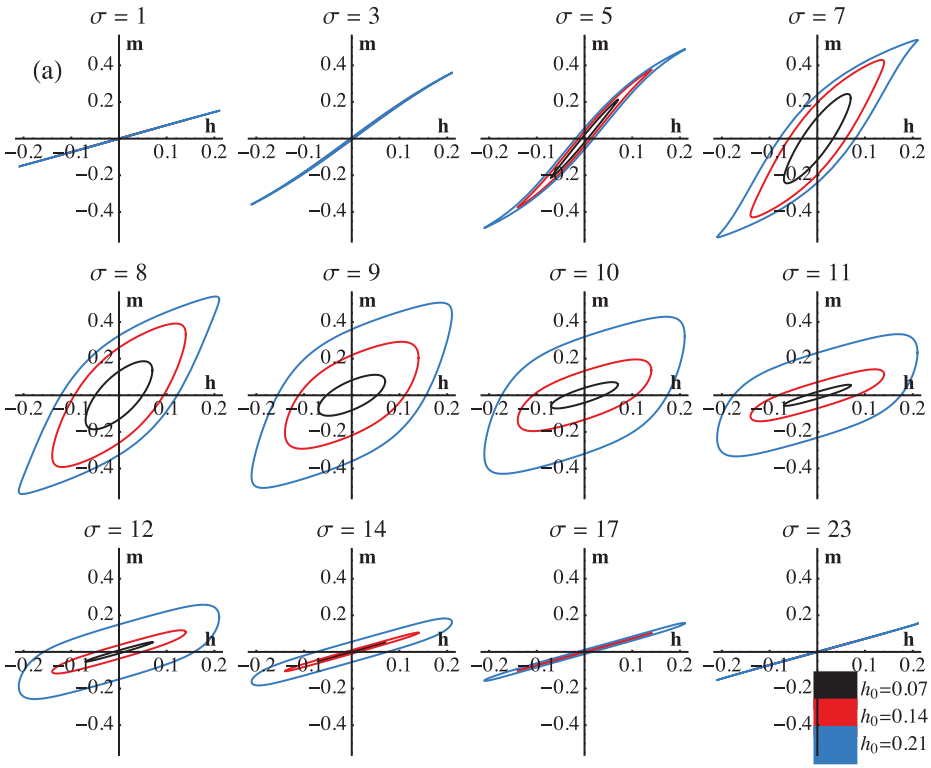

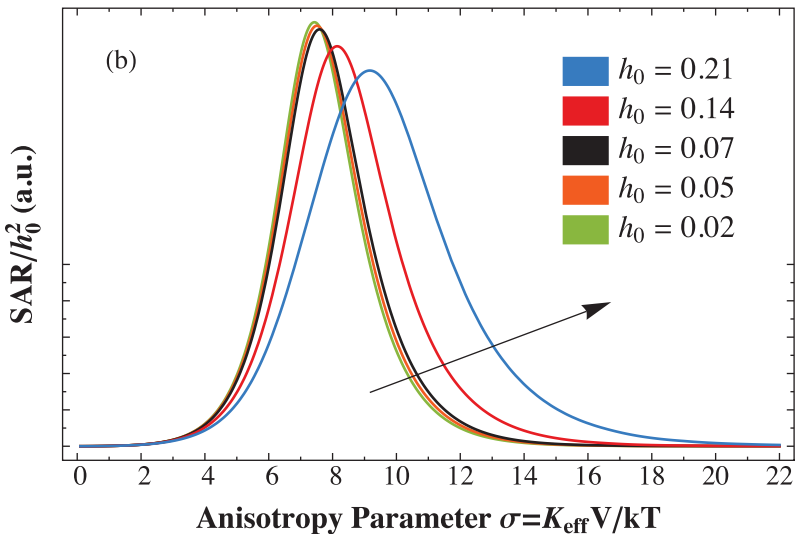

FIG. 7. (a) Dynamic hysteresis simulations calculated from Eq. (3) with f = 500 kHz, $\tau_0 = 5 \times 10^{-10}$ s and $\alpha = 1$ and different values of the anisotropy parameter σ and dimensionless magnetic field h_0. (b) SAR/h_0^2 vs. σ for different values of h_0.

V. CONCLUSIONS

In conclusion, we investigated in detail the influence of several key parameters of cobalt-ferrite nanoparticles on the specific absorption rate for magnetic hyperthermia applications. The nanoparticles were synthesized by a coprecipitation method and analyzed using x-ray diffraction and Rietveld analysis. Their sizes were inferred to lie between 3 and 14 nm, with most samples having an inverted spinel structure. The magnetic parameters were extracted from static magnetization data which showed that both the saturation magnetization and the coercivity increase with increasing particle size. The effective anisotropy was obtained from the coercivity by considering a three dimensional random anisotropy axis model taking into account particle-particle interactions.

The magneto-thermal (magnetic hyperthermia) properties of the powder samples were performed at 500 kHz for a field range up to 68 Oe. The specific absorption rate was found to increase quadratically with the magnetic field, as predicted by the linear response theory. We have also shown that the dimensionless parameter $\sigma = K_{ef}V/kT$ encompasses several key properties of the system and greatly simplifies the interpretation of the experimental data. We have also compared our results with the predictions of the linear response theory and showed that, if one includes the particle size distribution, exceptional agreement can be found. In

particular, both predict a maximum for the SAR close to $\sigma_m = 7.2 \pm 0.9$. These results indicate that, unlike the saturation magnetization, the anisotropy need to be carefully tailored in order to optimize the materials properties for hyperthermia applications. Finally, we discussed the transition from the linear to the non-linear regime as the field amplitude is increased by means of numerical simulations of dynamic hysteresis. From this analysis, it becomes quite evident how non-linear contributions to the magnetization dynamics transform the hysteresis loops. This approach, which is based on the stochastic Landau-Lifshitz equation, has shown to be quite robust, enabling one to investigate other aspects in detail, as for instance, the role of damping factor, magnetic anisotropy, field frequency, saturation magnetization, among other parameters.

ACKNOWLEDGMENTS

The authors would like to thank financial support from the Brazilian agencies CNPq, CAPES, FINEP, FAPEG, FAPESP, FAPDF, and FUNAPE. We also thank LNLS for the use of synchrotron facility to obtain the x-ray diffraction patterns of the samples.

[1]K. M. Krishnan, IEEE Trans. Magn. **46**, 2523 (2010).
[2]R. K. Gilchrist, R. Medal, W. D. Shorey, R. C. Hanselman, J. C. Parrot, and C. B. Taylor, Ann. Surg. **146**, 596 (1957).
[3]A. Jordan, R. Scholz, P. Wust, H. Fahling, J. Krause, W. Wlodarczyk, B. Sander, T. Vogl, and R. Felix, Int. J. Hyperthermia **13**, 587–605 (1997).
[4]M. H. A. Guedes, N. Sadeghiani, D. L. G. Peixoto, J. P. Coelho, L. S. Barbosa, R. B. Azevedo, S. Kückelhaus, M. F. Da Silva, P. C. Morais, and Z. G. M. Lacava, J. Magn. Magn. Mater. **293**, 283 (2005).
[5]A. Ito, H. Honda, and T. Kobayashi, Cancer Immunol. Immunother. **55**, 320 (2006).
[6]C. L. Dennis, A. J. Jackson, J. A. Borchers, P. J. Hoopes, R. Strawbridge, A. R. Foreman, J. van Lierop, C. Grüettner, and R. Ivkov, Nanotechnology **20**, 395103 (2009).
[7]B. Thiesen and A. Jordan, Int. J. Hyperthermia **24**, 467 (2008).
[8]W. Andrä, C. G. d'Ambly, R. Hergt, I. Hilger, and W. A. Kaiser, J. Magn. Magn. Mater. **194**, 197 (1999).
[9]R. E. Rosensweig, J. Magn. Magn. Mater. **252**, 370 (2002).
[10]A. S. Eggeman, S. A. Majetich, D. Farrel, and Q. A. Pankhust, IEEE Trans. Magn. **43**, 2451 (2007).
[11]C. G. Hadjipanayis, M. J. Bonder, S. Balakrishnan, X. Wang, H. Mao, and G. C. Hadjipanayis, Small **11**, 1925 (2008).
[12]J. Carrey, B. Mehdaoui, and M. Respaud, J. Appl. Phys. **109**, 083921 (2011).
[13]W. F. Brown, Jr., Phys. Rev. **130**, 1677 (1963).
[14]I. S. Poperechny, Yu. L. Raikher, and V. I. Stepanov, Phys. Rev. B **82**, 174423 (2010).
[15]G. T. Landi, J. Appl. Phys. **111**, 043901 (2012).
[16]S. M. Morgan and R. H. Victora, Appl. Phys. Lett. **97**, 093705 (2010).
[17]H. E. Mrabti, S. V. Titov, P. M. Dejardin, and Y. P. Kalmykov, J. Appl. Phys. **110**, 023901 (2011).
[18]Q. Zeng, I. Baker, J. A. Loudis, Y. Liao, P. J. Hoopes, and J. B. Weaver, Appl. Phys. Lett. **90**, 233112 (2007).
[19]A. V. Ramos, M. J. Guittet, J. B. Moussy, R. Mattana, C. Deranlot, F. Petroff, and C. Gatel, Appl. Phys. Lett. **91**, 122107 (2007).
[20]H. Zheng, J. Wang, S. E. Lofland, Z. Ma, L. M. Ardabili, T. Zhao, L. S. Riba, S. R. Shinde, S. B. Ogale, F. Bai, D. Viehland, Y. Jia, D. G. Schlom, M. Wuttig, A. Roytburd, and R. Ramesh, Science **303**, 661 (2004).
[21]Y. Wu, J. G. Wan, J. M. Liu, and G. Wang, Appl. Phys. Lett. **96**, 152902 (2010).
[22]E. A. S. Sikma, H. M. Joshi, Q. Ma, K. W. MacRenaris, A. L. Eckermann, V. P. Dravid, and T. J. Meade, Chem. Mater. **23**, 2657 (2011).
[23]K. Yosida and M. Tachiki, Prog. Theor. Phys. **17**, 331 (1957).
[24]V. A. M. Brabers, Phys. Rev. Lett. **68**, 3113 (1992).
[25]C. R. Alves, R. Aquino, J. Depeyrot, T. A. P. Cotta, M. H. Sousa, F. A. Tourinho, H. R. Rechenberg, and G. F. Goya, J. Appl. Phys. **99**, 08M905 (2006).
[26]M. Verveka, Z. Jirak, O. Kaman, K. Knizek, M. Marysko, E. Pollert, K. Zaveta, A. Lancok, M. Dlouha, and S. Vratislav, Nanotechnology **22**, 345701 (2011).
[27]J. M. Vargas, A. Srivastava, A. Yourdkhani, L. Zaldivar, G. Caruntu, and L. Spinu, J. Appl. Phys. **110**, 064304 (2011).
[28]M. Veverka, P. Veverka, O. Kaman, A. Lancok, K. Zaveta, E. Pollert, K. Knizek, J. Bohacek, M. Benes, P. Kaspar, E. Duget, and S. Vasseur, Nanotechnology **18**, 345704 (2007).
[29]D. H. Kim, D. E. Nickles, D. T. Johnson, and C. S. Brazel, J. Magn. Magn. Mater. **320**, 2390 (2008).
[30]H. M. Joshi, Y. P. Lin, M. Aslam, P. V. Prasad, E. A. S. Sikma, R. Edelman, T. Meade, and V. P. Dravid, J. Phys. Chem. C **113**, 17761 (2009).
[31]M. A. G. Soler, E. C. D. Lima, S. W. Silva, T. F. O. Melo, A. C. M. Pimenta, J. P. Sinnecker, R. B. Azevedo, V. K. Garg, A. C. Oliveira, M. A. Novak, and P. C. Morais, Langmuir **23**, 9611 (2007).
[32]R. Itri, J. Depeyrot, F. A. Tourinho, and M. H. Sousa, Eur. Phys. J. E **4**, 201 (2001).
[33]J. A. Gomes, M. H. Sousa, G. J. Silva, F. A. Tourinho, J. Mestnik-Filho, R. Itri, G. M. Azevedo, and J. Depeyrot, J. Magn. Magn. Mater. **300**, e213 (2006).
[34]J. G. Otero, A. J. G. Bastida, and J. Rivas, J. Magn. Magn. Mater. **189**, 377 (1998).
[35]B. D. Cullity and C. D. Grahan, *Introduction to Magnetic Materials* (John Wiley & Sons, New York, 2009).
[36]A. F. Bakuzis, P. C. Morais, and F. A. Tourinho, J. Magn. Reson. **122**, 100 (1996).
[37]A. F. Bakuzis, P. C. Morais, and F. Pelegrini, J. Appl. Phys. **85**, 7480 (1999).
[38]V. P. Shilov, Yu. L. Raikher, J. C. Bacri, F. Gazeau, and R. Perzynski, Phys. Rev. B **60**, 11902 (1999).
[39]L. Kumar and M. Kar, J. Magn. Magn. Mater. **323**, 2042 (2011).
[40]L. L. Castro, G. R. R. Gonçalves, K. Skeff Neto, P. C. Morais, A. F. Bakuzis, and R. Miotto, Phys. Rev. E **78**, 061507 (2008).
[41]E. R. Cintra, F. S. Ferreira, J. L. Santos, Jr., J. C. Campello, L. M. Socolovsky, E. M. Lima, and A. F. Bakuzis, Nanotechnology **20**, 045103 (2009).
[42]M. T. A. Eloi, J. L. Santos, Jr., P. C. Morais, and A. F. Bakuzis, Phys. Rev. E **82**, 021407 (2010).
[43]J. A. Gomes, M. H. Sousa, F. A. Tourinho, R. Aquino, G. J. Silva, J. Depeyrot, E. Dubois, and R. Perzynski, J. Phys. Chem. C **112**, 6220 (2008).